Received: 3 August 2021, Accepted: 14 October 2021, Published: 31 May 2022, Publisher: UTP Press, Creative Commons: CC BY 4.0

# GLYCEROL-MEDIATED SYNTHESIS OF NITROGEN-DOPED $TiO_2$ WITH EXCELLENT ADSORPTION AND PHOTOCATALYTIC ACTIVITY FOR REMAZOL RED DYE REMOVAL

**Paveethra Selvaraj, Rab Nawaz*, Nurul Tasnim Sahrin & Chong Fai Kait**

Fundamental and Applied Sciences Department, Universiti Teknologi PETRONAS, Malaysia
Center of Innovative Nanostructures and Nanodevices, Institute of Autonomous System, Universiti Teknologi PETRONAS, Malaysia

*Email: *rabnawaz.utp@gmail.com

## ABSTRACT

*This paper reports the synthesis, characterization, and application of nitrogen-doped $TiO_2$ (N-$TiO_2$) as an adsorbent and photocatalyst for the removal of Remazol Red Dye (RRD) from aqueous solution. The N-$TiO_2$ was prepared via a sol-gel technique using glycerol and water as solvent mixture and urea as N-precursor. The effect of N:Ti molar ratio (15:1, 20:1, and 25:1) and calcination temperature (300, 400, and 500°C) was evaluated on the structural, morphological, optical, and electronic, textural properties as well as the photocatalytic performance of the N-$TiO_2$ nanomaterials. The results demonstrated that the N:Ti molar ratio plays an important role in the formation of crystalline N-doped $TiO_2$ photocatalysts. All the synthesized N-$TiO_2$ were anatase phase with enhanced visible light absorption, displaying narrow bandgaps (2.64-2.50 eV), small particle sizes ranging from 23.1-25.2 nm, and specific surface area ranging from 72.33 to 252.69 $m^2/g$. The N:Ti molar ratio and calcination temperature play a crucial role in pre-equilibrium adsorption and photocatalytic removal of RRD. The N-$TiO_2$ with N:Ti molar ratio of 25:1 was able to remove 95.85% of RRD was compared to merely 36.06% by the N:Ti, 15:1, within 30 min of the adsorption process. However, the photocatalytic removal by N:Ti, 15:1 of RRD was drastically enhanced to 100% within 30 min of photoreaction compared to 99.44% by N:Ti, 25:1. The RRD removal via adsorption by N:Ti, 25:1 was increased from 36.06% to 78.53% and 96.05%, increasing calcination temperatures from 300 to 400 and 500°C, respectively. The RRD removal via photocatalysis was 87.30%, 97.41 and 99.44% when the photocatalyst was calcined at 300, 400 and 500°C, respectively. The outcome of this work suggests that N-$TiO_2$ has good potential when employed as an adsorbent and photocatalyst for RRD removal from textile wastewater.*

***Keywords:*** *adsorption, Nitrogen-doped $TiO_2$, photodegradation, remazol red dye*

## INTRODUCTION

The textile industry plays a phenomenal role in the economic prosperity of a nation but at the expense of environmental deterioration. Textile wet processing, including dyeing, printing and chemical finishing, produces a huge amount of liquid effluent. If discharged untreated can cause severe water pollution because of the synthetic origin of the dyes and the complex molecular structure that makes them resilient to degradation [1]-[2]. The most widely used dyes in the textile industry are the reactive fiber dyes like Remazol Red Dye (RRD) and the amount of the dyes used ranges from 10%-50%. The discharge of such effluent loaded with RRD could be detrimental to human health and the aquatic ecosystem. Despite the efforts by various textile industries to treat its liquid effluent to comply with the stipulated standard discharge limit, the traditional treatment systems are reported to be inefficient for the removal of organic dyes from textile wastewater [3]. Therefore, advanced treatment is required to remove the

RRD from textile wastewater before letting it enter the environment.

Amongst the treatment approaches, adsorption is the most popular method for organic dye removal from wastewater originating from the textile industry. Various adsorbents such as activated carbon [4], carbon nanotubes, chitin, chitosan, clays, coal, silica and zeolite have been investigated for the removal of organic dyes from wastewater [4]-[6]. However, the high cost of adsorbents compelled researchers to look for alternative adsorbents that are cheaper and more stable in actual wastewater [7]. $TiO_2$ metal oxide, in combination with other carbon-based materials such as activated carbon or graphene, has been reported to improve the adsorptive properties of $TiO_2$ [8]. However, $TiO_2$ as a standalone adsorbent has been rarely reported in the literature. Therefore, investigation of $TiO_2$ as an adsorbent for the removal of organic dyes can be a viable approach and is anticipated to enhance performance because of its suitable physicochemical properties.

When used as a photocatalyst, the pure or modified $TiO_2$ has shown higher degradation efficiency for organic dyes, which have been proven in previous studies [1]-[2], [9]-[10]. However, most previous studies used UV light as the energy source. Using visible light instead of UV light could be a more promising and economically viable approach as solar radiation consists of 45% of the visible light portion, which is abundantly available free of charge. Various strategies such as metal doping, nonmetal doping, dye sensitization, and organic coating has been devised to enhance the absorption of visible light by $TiO_2$. Amongst them, nonmetal doping has proven to display greater potential to increase visible light absorption, reduce the bandgap and improve the performance of $TiO_2$ for the degradation of a variety of organic compounds [11]-[12]. The pathway of doping $TiO_2$ with nitrogen has attracted vast attention owing to its low cost, high efficacy and environmental friendliness [13]. However, it is crucial to devise an efficient and facile route for the synthesis of N-$TiO_2$ to improve visible light absorption and subsequent photocatalytic performance. As far as the authors are concerned, reports related to the glycerol-mediated synthesis of N-$TiO_2$ and its application as an adsorbent and photocatalyst for RRD removal is not available in the literature.

In this study, the N-$TiO_2$ materials were synthesized via a modified sol-gel method involving hydrolysis of $TiCl_4$ in an aqueous glycerol medium in the presence of urea as the N-source, followed by characterization using various techniques. The effect of N:Ti molar ratio and calcination temperature were investigated on adsorptive and photocatalytic properties and performance for the removal of RRD. A thorough characterization revealed that the synthesized N-$TiO_2$ were anatase phase, with a large specific surface area, improved visible light absorption, and narrow bandgap.

## EXPERIMENTAL

### Synthesis of N-$TiO_2$

The N-doped $TiO_2$ photocatalysts with different N:Ti molar ratios were synthesized via a modified sol-gel technique reported by Cheng et al. in 2016 [14]. The detailed synthesis conditions for N-doped $TiO_2$ are shown in Table 1, while its schematic illustration of the synthesis is shown in Figure 1. Glycerol ($C_3H_8O_3$, 98%, Fischer Scientific) and deionized water was mixed in a fixed ratio of 9:1 (v/v) followed by the addition of a different amount of urea ($CH_4N_2O$, 99%, Merck) to obtain a different molar ratio of N: Ti. Titanium tetrachloride ($TiCl_4$, 99%, Merck) was added dropwise to the mixture to a final amount of 0.1 mol under constant stirring for hydrolysis to proceed. A 300 mL of 2.5 M aqueous ammonia ($NH_4OH$, 25%, Merck) was added dropwise to the solution to achieve the final pH of 10 for maximum precipitation. The sol was aged in ambient conditions for 24h under continuous stirring. Subsequently, the sol was dried for 24h in an oven at 70°C and then calcined at different calcination temperatures and durations with a heating rate of 5°C $min^{-1}$. $TiO_2$ photocatalyst was synthesized as a reference using the same procedure but without the addition of urea, followed by calcination at 300°C for 1h.

### Characterization of the N-$TiO_2$ Materials

The synthesized materials' crystalline structure, phase composition, and crystallite size were obtained using an x-ray diffractometer (PANalytical X'Pert$^3$ Powder) with Cu $K_\alpha$ radiation (40 kV, 40 mA). The scanning was carried out for $2\theta$ between 5°-80° with a scan step size of 0.026261°. The average crystallite sizes of the prepared materials were calculated using Scherrer's formula as

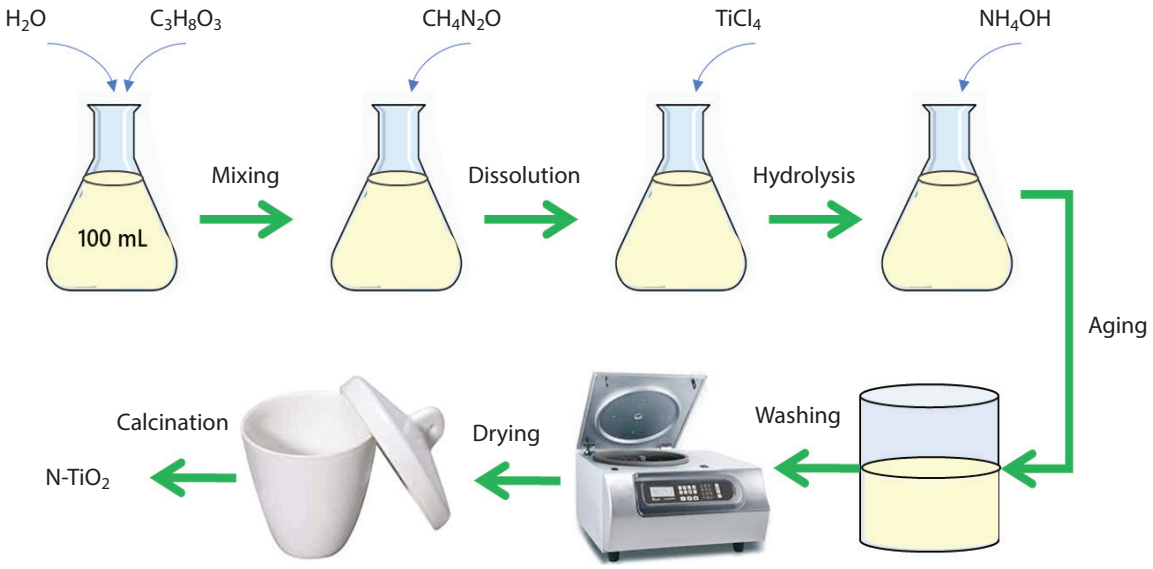


**Figure 1** Schematic illustration of the sol-gel synthesis of $N\text{-}TiO_2$.

**Table 1** Synthesis conditions and nomenclature of the $N\text{-}TiO_2$ photocatalysts

| Sample | N:Ti (molar ratio) | Calcination temperature (C°) | Calcination duration (h) |
|---|---|---|---|
| N:Ti (15:1) | 15:1 | 300 | 1 |
| N:Ti (20:1) | 20:1 | 300 | 1 |
| N:Ti (25:1) | 25:1 | 300 | 1 |
| N:Ti 400 | 25:1 | 400 | 1 |
| N:Ti 500 | 25:1 | 500 | 1 |
| N:Ti 2 | 25:1 | 300 | 2 |
| N:Ti 3 | 25:1 | 300 | 3 |

shown in Equation 1 from the characteristic diffraction peaks for the (101) plane of anatase $TiO_2$ at $2\theta = 25°$.

$$D = \frac{K\lambda}{\beta Cos\theta} \quad (1)$$

where, $D$ is the average crystallite size (nm), $K$ is the Scherrer's constant (0.9), $\lambda$ is the Cu $K_\alpha$ radiation wavelength (0.15418 nm), $\beta$ is the full width at half maximum (FWHM) of the selected diffraction peak in radian and $\theta$ is the Bragg's diffraction angle.

XPS data were collected using a Thermo-Fischer Scientific spectrometer (K–Alpha, Madison, WI, USA) with C1s correction at 284.6 eV for calibration and Al Kα (1486.60 eV) as the x-ray excitation source. The peaks were deconvoluted and fitted using Gaussian curve fitting. Field emission scanning microscopy (FESEM) was used to examine the surface morphology of the synthesized materials. The FESEM images were captured at 50 kX magnification using a Carl Zeiss instrument (SUPRA 55VP) at an acceleration voltage of 30 kV. The diffuse reflectance UV-Visible (DRUV-Vis) spectra of the samples were obtained in the UV-Visible region ($\lambda$ = 200-800 nm) using a UV-Vis spectrometer (Agilent Carry100, Santa Clara, CA, USA) with Spectralon as the reference material. The adsorption isotherms of the samples were acquired at –195°C using Micromeritics ASAP 2020 analyzer (Micromeritcs Corps., Norcross, GA, USA). Before measurements, the samples were degassed and the specific surface area of the sample was calculated based on Brunauer, Emmett and Teller (BET) method from the adsorption measurement. The pore size of the sample was calculated from desorption data using Barrett-Joyner-Halenda (BJH) method.

### Adsorption and Photocatalytic Performance

The experimental setup for carrying out adsorption and photocatalytic performance is displayed in Figure 2. A fixed amount of $N\text{-}TiO_2$ (0.05 g) with different N:Ti molar ratios was suspended in 120 mL aqueous RRD solution (10 mg/L initial concentration) in a 250 mL jacketed Pyrex® photoreactor and vigorously stirred in the dark. After 30 min, a sample was withdrawn from the photoreactor and filtered prior to analysis.

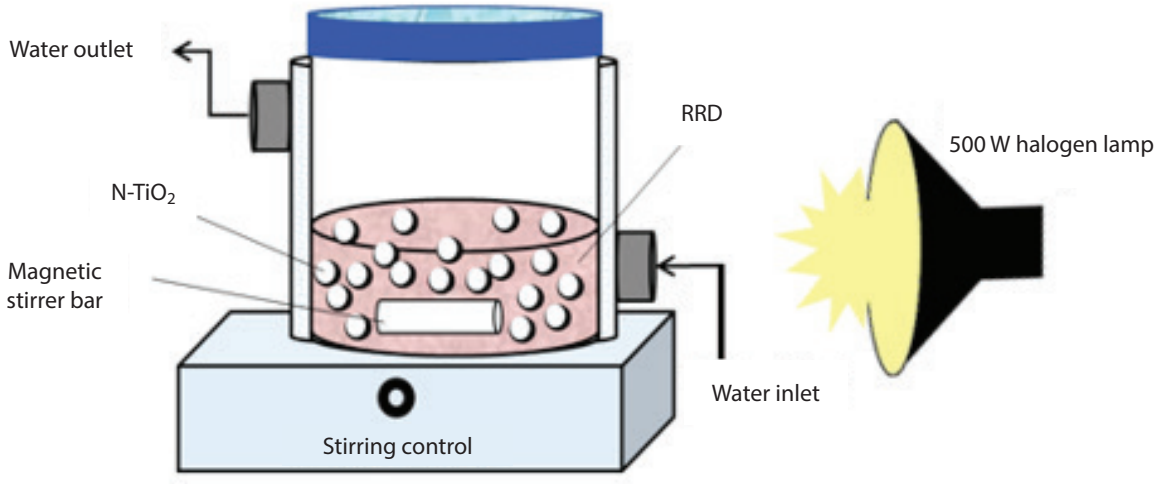


**Figure 2** The experimental setup for carrying out adsorption and photocatalytic tests

The RRD removal via adsorption was calculated using Equation 2.

After the initial 30 min dark phase to achieve the adsorption-desorption equilibrium, the RRD aqueous solution was irradiated with visible light irradiation from a 500 W halogen lamp. Water was continuously circulated through the jacketed vessel to regulate the temperature of the reaction media. Vigorous stirring was maintained during the photoreaction to ensure homogenization of the N-$TiO_2$ in the RRD solution. Samples were withdrawn from the photoreactor at a selected duration of light radiation (15 min, 30 min and 60 min), filtered and the RRD concentration monitored. The RRD removal via adsorption and photocatalysis was monitored from the maximum absorption peak at 519 nm using SpectroVis plus instrument. The adsorptive and photocatalytic removal of RRD was estimated using Equation 2.

$$RRD\ removal\ (\%) = \frac{C_o - C_t}{C_o} \times 100\% \qquad (2)$$

where $C_o$ is the initial concentration and $C_t$ is the concentration of RRD at any given time of sampling interval during the dark phase and light radiation.

## RESULTS AND DISCUSSION

### Properties of the N-$TiO_2$

XRD patterns of all the synthesized N-$TiO_2$ were analyzed to determine the effect of N:Ti molar ratio, calcination temperature and calcination duration on the crystalline structure. The XRD patterns, as displayed in Figure 3a, revealed that all the synthesized N-doped $TiO_2$ samples are anatase phase, as suggested by the presence of a characteristic peak at $2\theta = 25°$ matching well with the anatase plane (101) and good agreement with previous studies [15]. No phase transformation from anatase to rutile or brookite crystalline phases was observed with the increase in N:Ti molar ratio, calcination temperature or calcination duration. It should be noted that the diffraction peaks of the Ni:Ti (25:1) become more intense and sharper compared to the sample with lower N:Ti molar ratios of 15:1, and 20:1, indicating that N:Ti molar ratio plays an important role in the crystallization of the N-doped $TiO_2$.

The other diffraction peaks corresponding to the (002) plane of the anatase phase were not present in the XRD patterns during the crystallization of the N-$TiO_2$, although it has been reported elsewhere [16]. This can be explained by the lower calcination temperature or the calcination in the oxygen atmosphere compared to the higher temperature and $N_2$ atmosphere reported in previous studies [15],[17]. As shown in Figure 3b, when the calcination temperature was increased to 400 and 500°, the other diffraction peaks corresponding to the anatase phase started to appear in the diffractogram.

The effect of calcination temperature and calcination duration on the structural properties, including the crystalline structure and phase composition of the N:$TiO_2$ was investigated. It was found that calcination

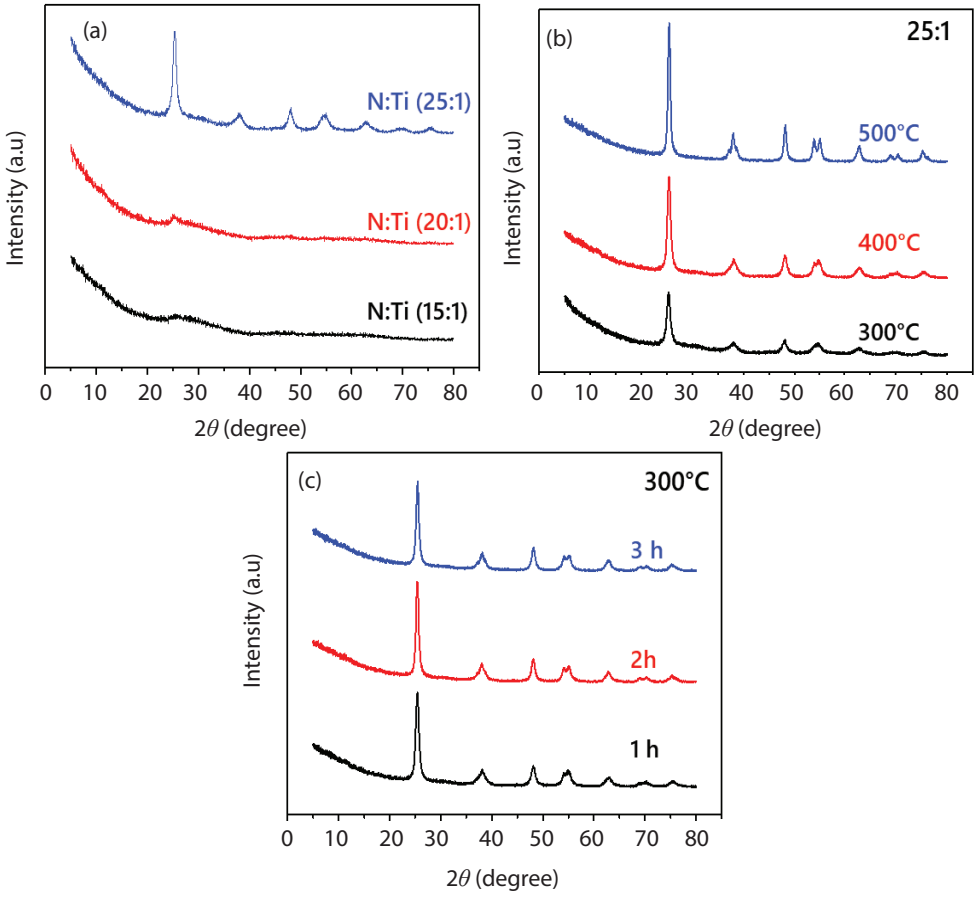


**Figure 3** XRD patterns of the N-$TiO_2$ at different (a) N:Ti molar ratios, (b) calcination temperatures (N:Ti = 25:1), and (c) calcination durations (N:Ti = 25:1)

temperature significantly affects the crystallinity of the N-doped $TiO_2$, as revealed by the XRD patterns shown in Figure 3b. The diffraction peaks at $2\theta = 25°$ become sharper when the calcination temperature is increased to 400 and 500°C. On the other hand, the calcination duration did not significantly affect the crystalline phase or crystallization of the N:Ti (20:1). The average crystallite size calculated using Scherrer's equation increased from 8.53 nm to 28.45 nm, increasing N:Ti molar ratio from 15:1 to 25:1. The average crystallite size of the N:Ti (20:1) also increased with increasing calcination temperature and calcination duration. The increase in calcination temperature was expected to increase the crystallite size because of the inter-agglomeration of the crystallites at a higher temperature.

The FESEM micrographs shown in Figure 4a–4c revealed that the N-doped $TiO_2$ samples with N:Ti ratios of 15:1, 20:1 and 25:1 are spherical shaped nanosized particles. The results demonstrate that N:Ti molar ratio has no significant effect on the morphology of the $TiO_2$ photocatalyst. The particle size of the samples was estimated randomly from 200 selected particles using image-J software. The particle size distribution was estimated using Gaussian line fitting and the results are shown in Figure 4d-4f. The average particle diameter was 25.17 nm at N:Ti molar ratio of 15:1, whereas it was decreased to 24.70 nm when the N:Ti molar was increased to 25:1.

The XPS investigations were carried out to determine the elemental composition and chemical environment of the synthesized N-$TiO_2$. The XPS survey spectra of the samples are shown in Figure 5a. The survey spectra confirm N's presence in the crystal lattice of the N-$TiO_2$. The high-resolution Ti2p orbital scan of the N-$TiO_2$ samples are shown in Figure 5b. The sample N:Ti (15:1), presented orbital doublet peaks corresponding to $Ti2p_{3/2}$ and $Ti2p_{1/2}$ at a binding energy of 459.79 and

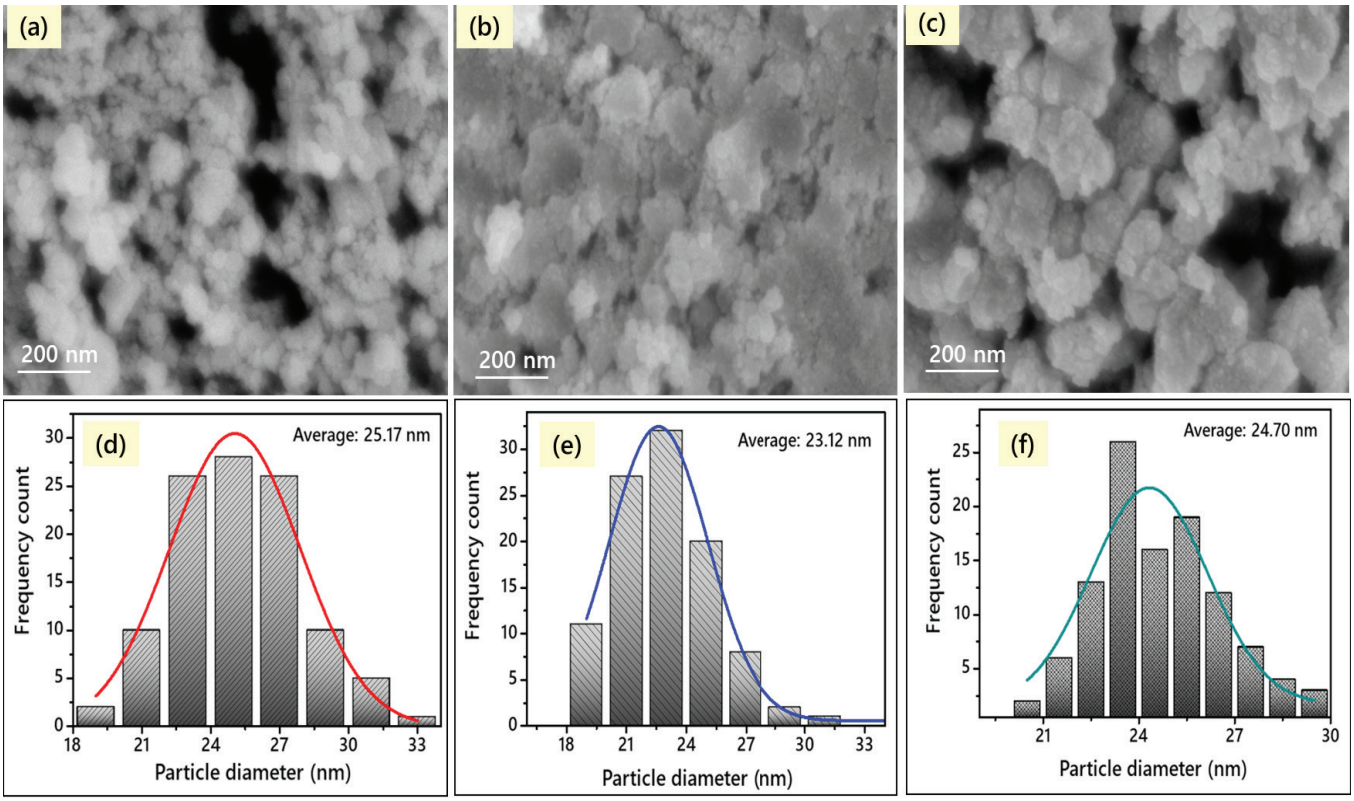


**Figure 4** FESEM micrographs of (a) N:Ti (15:1), (b) N:Ti (20:1), and (c) N:Ti (25:1), and particles size distribution of (d) N:Ti (15:1), (e) N:Ti (20:1), and (f) N:Ti (25:1)

465.45 eV, respectively which is slightly higher than the theoretical values of anatase $TiO_2$. The Ti2p orbital doublet peaks of N:Ti (20:1) shifted to the lower binding energy of 459.35 and 465.03 eV. The shift to lower binding energy could be due to the replacement of $O^{2-}$ with $N^{3-}$ which led to the formation of Ti-N bonding and thus resulted in an increase in the electron density on Ti due to the introduction of lower electronegative N ions [18]. This result confirms the substitution of oxygen with N in the lattice of $TiO_2$. On the other hand, the Ti2p doublet orbital peaks of N:Ti (25:1) shifted to higher binding energy, suggests a different chemical environment of the N-$TiO_2$ samples. The shift of the $Ti2p_{3/2}$ and $Ti2p_{1/2}$ peaks to 460.79 and 465.24 eV, respectively, in N:Ti (25:1) to higher binding energy can be due to the substitutional N affected by the proximity of $N_2$ molecules, which also evidenced the predominant formation of the $N_2$ in the material [19].

The Ti2p XPS results are consistent with the O1s peaks of the samples. The O1s spectra of the N-$TiO_2$ are presented in Figure 5c. The N-$TiO_2$ with a lower N:Ti ratio (15:1) presented the O1s peak located at a binding energy of 531.13 eV, whereas the O1s peak of the N:Ti (20:1) shifted to the lower binding energy of 530.7 eV. The shift in the binding energy of the O1s peak suggests that the oxygen vacancies were created in the sample as a result of charge compensation. On the other hand, the O1s peak of N:Ti (25:1) showed a positive shift and the peaks are now located at a higher binding energy of 531.98 eV. The deconvoluted N1s spectra of the N:Ti (15:1) shown in Figure 5d revealed three fitted peaks around 400.57, 402.0, and 403.55 eV, which can be attributed to the characteristic Ti-O-N, O-Ti-N and Ti-N bond linkages, respectively [20]. The sample N:Ti (20:1) did not show Ti-N bond linkage where the BE value of the N-bond linkages was shifted to a higher BE of 402.18 and 404.35 eV in N:Ti (25:1). The shift to higher BE can be explained on the basis of the evolution of Oxygen Vacancies (OVs) in the N-doped $TiO_2$ sample. The increase in OVs favors decreasing interstitial doping more than substitutional doping and the higher the number of OVs, the more substitutional doping compared to interstitial [17]. The peaks at higher binding energy (>402 eV) can also be attributed to unoccupied N2p states hybridized with the crystal field split Ti3d bands ($t_{2g}$ and $e_g$) are partially overlapped by a very narrow

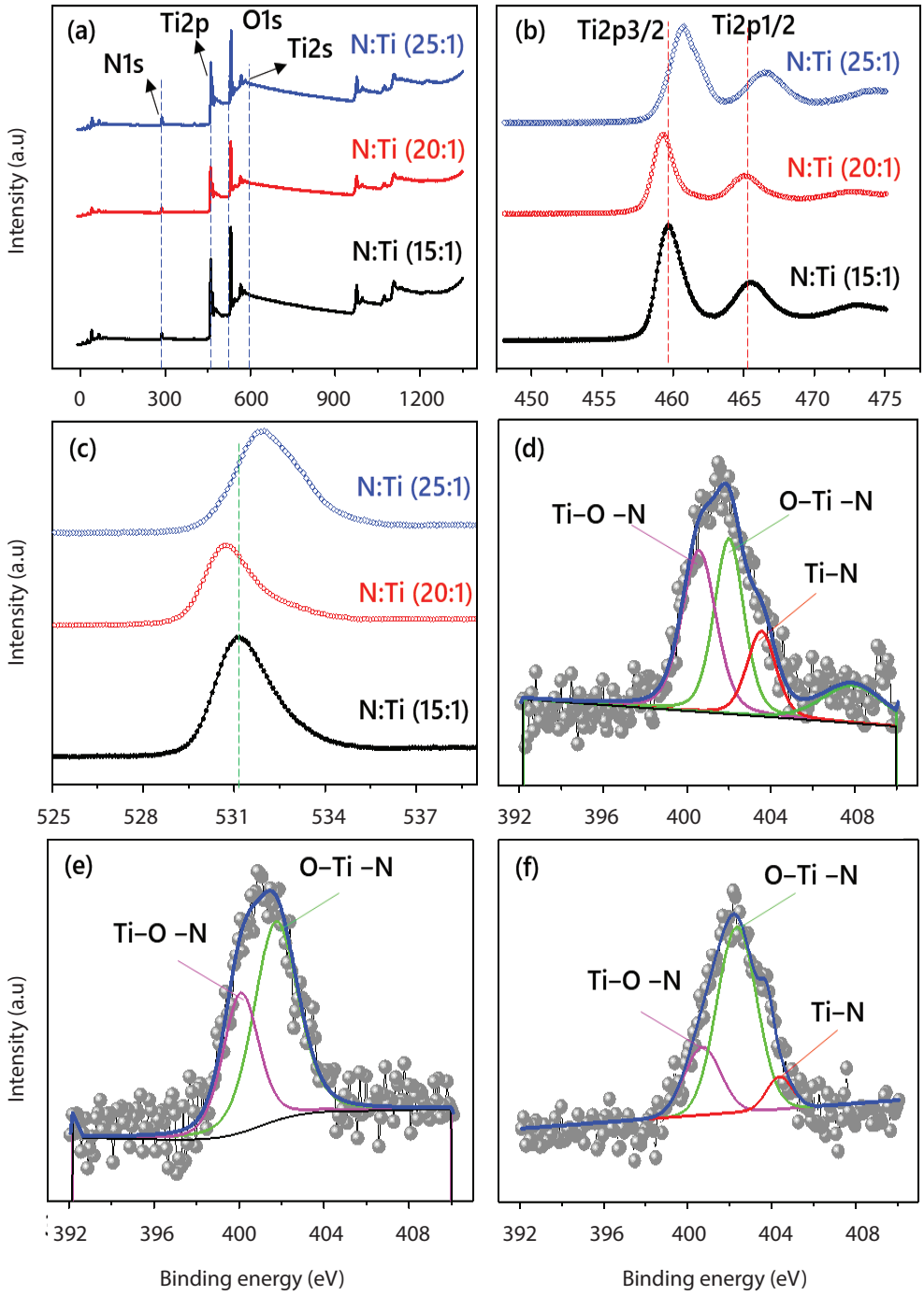


**Figure 5** (a) XPS survey spectra, (b) Ti2p XPS spectra, (c) O1s XPS spectra of the Ni:Ti (15:1), Ni:Ti (20:1), Ni:Ti (25:1) and high resolution deconvoluted N1s spectra of (d) Ni:Ti (15:1), (e) Ni:Ti (20:1), and (f) Ni:Ti (25:1)

peak [21]. The different kinds of interstitial dopants, i.e., N atoms in an interstitial position and interacting with various numbers of Ti neighbors, could lead to a peak broadening.

The bandgap ($E_g$) of the N-doped $TiO_2$ samples were calculated using the Tauc plot, based on the relation $(ahv)^2 = k(hv\text{-}E_g)$, where $hv$ is the energy of the incident light in eV, $k$ a constant and $\alpha$ is the absorption coefficient relationship. The bandgap of the undoped $TiO_2$ was 2.96 eV, and it was monotonically decreased to 2.69, 2.50, and 2.61 eV with increasing N:Ti molar ratio to 15:1, 20:1 and 25:1, respectively. The results suggest that the N:Ti molar ratio has no significant

effect on the valence band and conduction band of the N-$TiO_2$. However, the bandgap shows a significant reduction with an increasing N:Ti molar ratio, which indicates that the bandgap of N-$TiO_2$ samples reduced to the impurity level in the bandgap. The different N:Ti molar ratios may influence the absorption ability and photocatalytic activity of the N-doped $TiO_2$ under visible light irradiation. The improved visible light absorption of N-$TiO_2$ was attributed to the formation of localized energy states in the bandgap of $TiO_2$ induced by N-doping. The localized states result in a reduction of the energy required for the excitation of electrons and consequently lead to a redshift of the absorption edge [22]. Due to N-doping, the impurity energy state was located at 0.14 eV (substitutional) and 0.73 eV (interstitial) at the top of the VB edge. According to the density of energy states, the valence bandwidth is at 4.5 eV, larger than the bandgap of $TiO_2$ (3.2 eV). This indicates that the electron might be excited from both the impurity state of N into the CB of $TiO_2$ and from the VB of $TiO_2$ into the impurity state of N under the light of sufficient energy because this state is partially unoccupied [23]-[24].

The nitrogen physisorption isotherms of the N-doped $TiO_2$ samples are shown in Figure 6. The desorption branch in the hysteresis loop is separated from the adsorption branch in the relative pressure (P/P) range of 0.4-0.9, 0.6-0.8, and 0.5-0.6 for N:Ti (15:1), N:Ti (20:1), and N:Ti (25:1), respectively. The isotherms of the N-doped $TiO_2$ samples were characteristic of type IV isotherms, indicating that the synthesized N-doped $TiO_2$ photocatalysts are mesoporous in nature. The isotherms confirm their mesoporosity by the narrow pore size distribution ranging from 4.008-10.1601 nm. The N:Ti (20:1) showed the highest specific surface

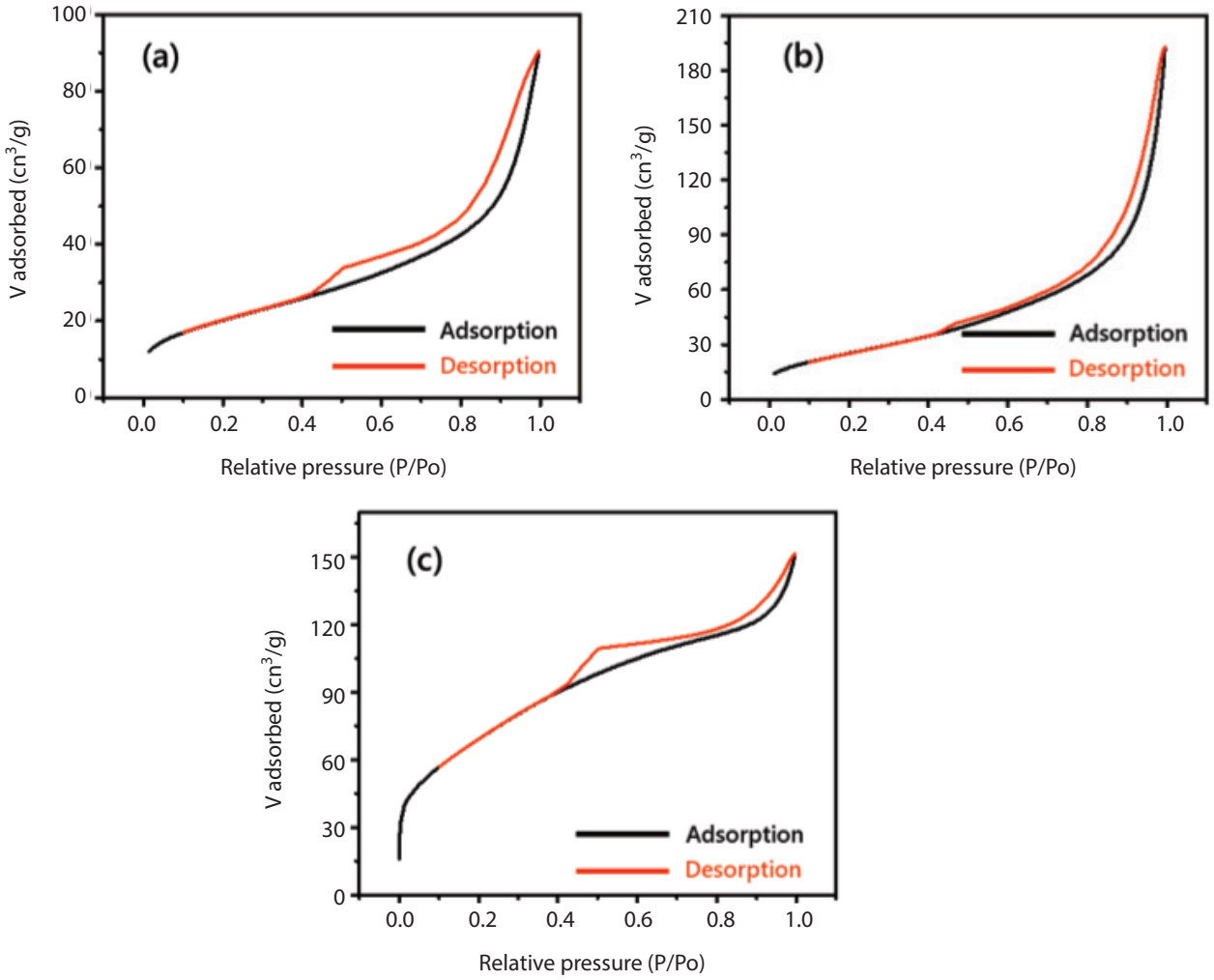


**Figure 6** Nitrogen physisorption isotherms of (a) N:Ti (15:1), (b) N:Ti (20:1), and (c) N:Ti (25:1)

area of 252.70 $m^2$/g. The other samples with lower and higher N:Ti molar ratios of 15:1 and 25:1 displayed a lower surface area of 72.33 and 93.72 $m^2$/g, respectively. Commonly, high surface area and rich pore structure are favorable to supply more active centers and high adsorption capacity towards pollutant molecules resulting in better photocatalytic activity [25].

**Adsorption and Photocatalytic Performance**

The adsorption and photocatalytic performance of the N-$TiO_2$ are shown in Figure 7. Reaction in the dark represents adsorption, while the reaction in light refers to photocatalysis. The normalized concentration of RRD after 30 min of adsorption reaction and 60 min of photocatalytic reaction under visible light irradiation is presented in Figure 7a. The percentage of RRD removed via adsorption and photocatalysis is displayed in Figure 7b. It was observed that the RRD adsorptive removal was enhanced with an increased N:Ti molar ratio. For instance, the RRD removal by adsorption increased from 36.06% to 78.53% and 96.05% when the N:Ti molar ratio increased from 15:1 to 20:1 and 25:1, respectively. Similarly, N:Ti (25:1) and calcined at 500°C showed better adsorption ability by removing more than 99% of the RRD within 30 min, as depicted in Figure 7d. The N:Ti (25:1) and calcined at 300 and 400°C showed only 35% and 76% RRD removal by adsorption. The adsorption capacities decreased with increasing treatment temperatures, corresponding to the changes in the specific surface area. As depicted in Figure 7c, the concentration of RRD reduced to almost 0 mg/L at N:Ti molar ratio of 25:1 and calcination of 500°C. The RRD removal via photocatalysis was more than 96% by N:Ti (25:1) and calcined at 300°C, as displayed in Figure 7). The increased removal of RRD by N:Ti (25:1)

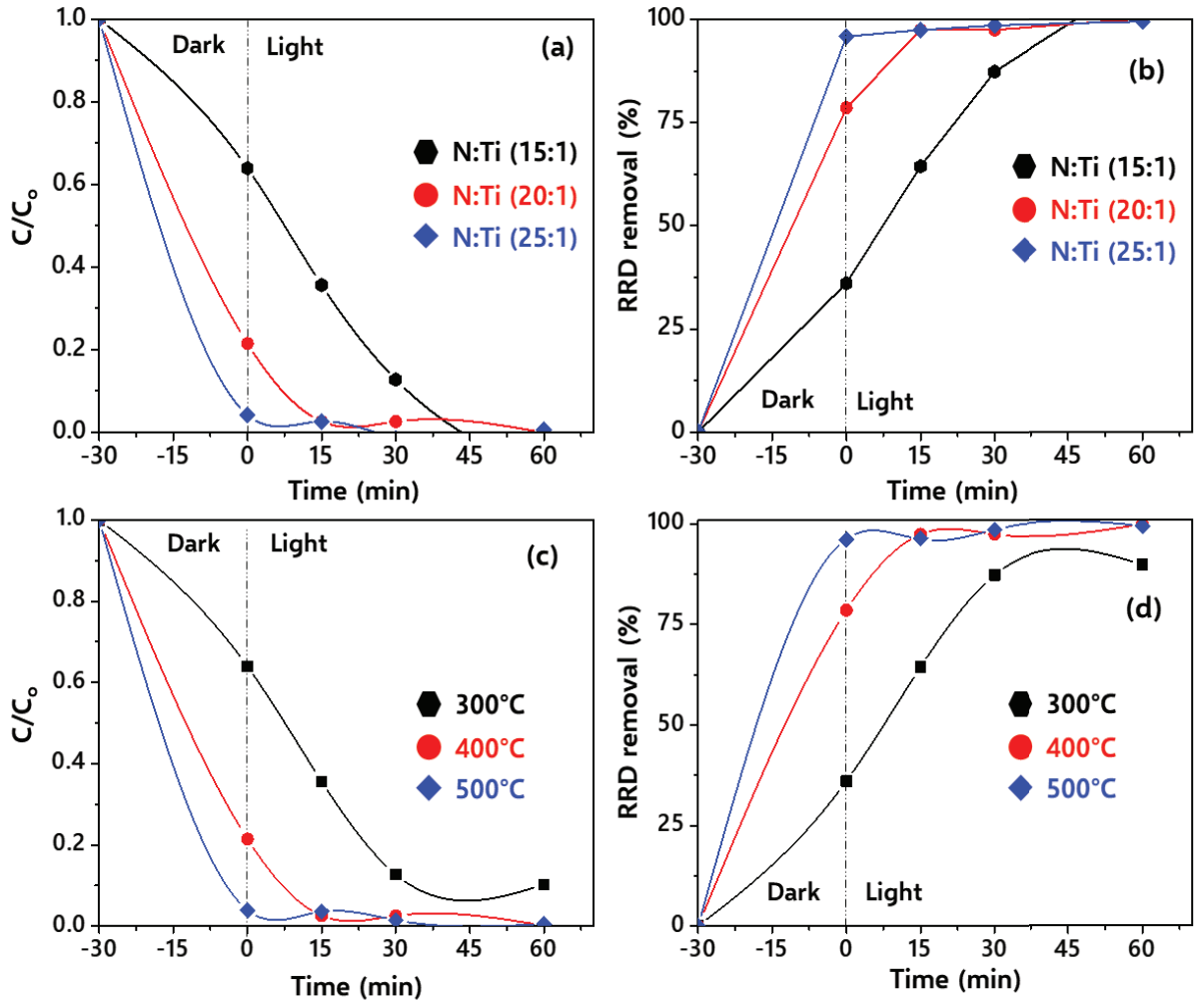


**Figure 7** Effect of N:Ti molar ratio on (a) Normalized concentration of RRD, (b) percentage removal of RRD; effect of calcination temperature on (c) normalized concentration of RRD, (d) percentage removal

could be due to its high crystallinity indicated by the sharp diffraction peaks of the XRD pattern in Figure 3a and this observation is consistent with previous literature [26]. The low adsorption and photocatalytic performance of the N:Ti (20:1) compared to N:Ti (25:1) could be due to the low crystallinity of N:Ti (20:1) which results in more crystal defects and consequent high electron-hole pair recombination. The improved crystallization of N:Ti (25:1) enhanced the separation efficiency of the photo-generated electrons and holes because of the reduced recombination center in bulk $TiO_2$ [27].

The adsorption of RRD on the $TiO_2$ surface is a prerequisite for photocatalytic reactions, and the greater specific surface area is generally favourable to yield the higher photocatalytic activity. However, photocatalytic activity does not depend only on the BET-specific surface area in photocatalytic removal of RRD. During the photocatalytic process, the adsorption ability and crystallinity of the catalyst are the main influence factors on the photocatalytic removal efficiency. In order to further identify the photocatalytic removal efficiency influenced by the crystallinity of $TiO_2$, Jiang et al. [28] proposed the intrinsic rate constant $k_{in}$ , which means excluding the influence of adsorption on the apparent first-order rate constant $k_{app}$, and the definition of the intrinsic rate constant $k_{in}$, which reflects the effect of the $TiO_2$ crystalline phases and crystallinity on the photocatalytic rate.

Finally, it can be summarized that the large specific surface area and the high crystallinity of $TiO_2$ are favorable for high photocatalytic activity.

Different N:Ti molar ratios resulted in different pore structures for the three samples, as shown in Figures 7a, 7b and 7c, leading to different adsorption amounts for RRD. The adsorption capacities increased with increasing N:Ti molar ratio, corresponding to the change in surface area and pore volume.

As shown in Figure 8, the adsorptive removal of RRD was 36.06%, whereas the photocatalytic removal was 51.24% by N:Ti (15:1). The adsorptive removal was lower compared to photocatalytic removal. However, the adsorptive removal of RRD increased with an increase in the N:Ti molar ratio. The adsorptive removal was enhanced to 78.53% from 36.06% when the N:Ti molar ratio increased from 15:1 to 20:1. On the other hand, the photocatalytic removal decreased from 51.24% to 18.88%, with an increase in N:Ti molar ratio. The adsorptive removal of RRD further increased to 95.85%, whereas photocatalytic removal decreased to only 2.68%. If we compare N:Ti (20:1) and N:Ti (25:1), we might find that the former possessed somewhat lower adsorption capacity although higher surface area. The decrease in photocatalytic removal of RRD could be due to the complete coverage of the active sites on the photocatalyst surface by adsorption of RRD, which is evident from the increase in adsorptive

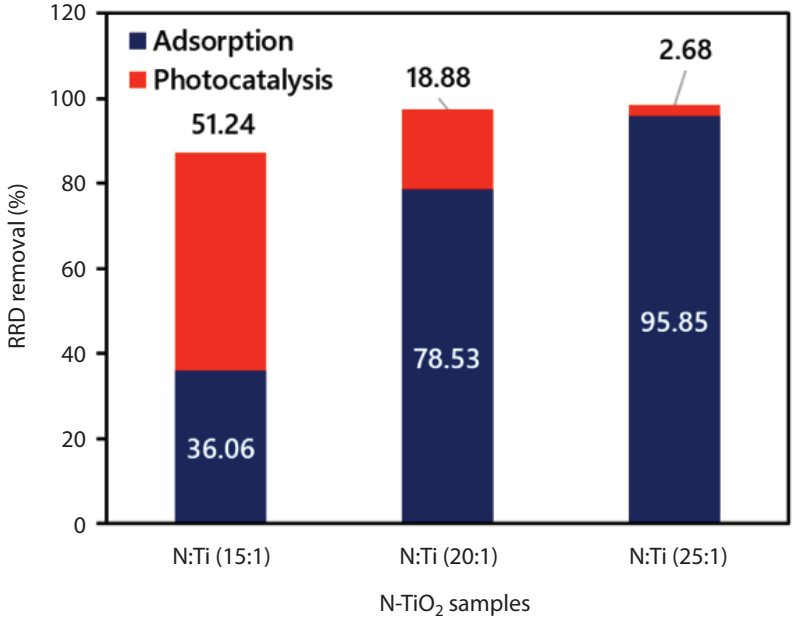


**Figure 8** Comparison of RRD removal by adsorption and photocatalysis using N-$TiO_2$

removal [29]. The decrease in photocatalytic removal can also be attributed to the number of RRD molecules available for the removal, as most RRD molecules were removed via adsorption. The dissimilar adsorption and photoreactivity of N-doped samples are not surprising because the adsorption and photocatalytic activity does not depend only on the crystallinity but on many other parameters, such as specific surface area, hydroxylation degree, surface acid and basic centres amount, zero charge point and the two samples have been prepared by different methods [30]. The results demonstrated excellent adsorption the photocatalytic capability of the N-$TiO_2$. Figures 7c and 7d revealed that calcination temperature significantly affects the adsorptive and photocatalytic removal of RRD from an aqueous solution. So, it can be inferred that the chemisorption dominated the RRD removal a process by the N-$TiO_2$ and the N-$TiO_2$ possessed great potential to be used in the textile industry for organic dye removal.

## CONCLUSION

Anatase phase nitrogen-doped $TiO_2$ was successfully produced via glycerol-assisted modified sol-gel technique. The glycerol and nitrogen play an important role in modifying the optical and electronic properties of the $TiO_2$. The N:Ti molar ratio and calcination temperature have no significant effect on the crystalline structure of the N-$TiO_2$. The crystallinity of the N-$TiO_2$ increased with increasing N:Ti molar ratio and calcination temperature. The synthesized N-$TiO_2$ showed a narrow bandgap of 2.61 eV and an enhanced surface area of 72.33 $m^2$/g. N-TiO2 removed more than 95% of RRD with N:Ti molar ratio of 25:1 within 30 min of dark reaction time. The adsorption followed by 30 min of photocatalytic reaction removed more than 99% of the initial 10 mg/L of RRD from the aqueous solution. The N-$TiO_2$ demonstrated excellent adsorption and photocatalytic removal for Remazol red dye removal.

## ACKNOWLEDGEMENT

The authors would like to thank the Centre of Innovative Nanostructures and Nanodevices (COINN) and Photocatalyst Laboratory at Catalyst Research (CARE) Laboratory in Universiti Teknologi PETRONAS for providing the facilities. Financial support from the Ministry of Higher Education Malaysia (FRGS/1/2020/STG05/UTP/02/2) and Yayasan Universiti Teknologi PETRONAS (YUTP 015LC0-276) are greatly acknowledged.

## REFERENCES

[1] M. Asiltürk, F. Sayılkan, F.S. Erdemoğlu, S.M. Akarsu, H. Sayılkan, M. Erdemoğlu & E. Arpaç, "Characterization of the hydrothermally synthesized nano-$TiO_2$ crystallite and the photocatalytic degradation of Rhodamine B", *Journal of Hazardous Materials,* 129, 1-3, pp. 164-170, 2006. Doi:10.1016/j.jhazmat.2005.08.027

[2] N. Riaz, F.K. Chong, B.K. Dutta, Z.B. Man, M.S. Khan & E. Nurlaela, "Photodegradation of Orange II under visible light using Cu–Ni/$TiO_2$: Effect of calcination temperature", *Chemical Engineering Journal,* 185-186, pp. 108-119, 2012. Doi:10.1016/j.cej.2012.01.052.

[3] A. Hassani, L. Alidokht, A.R. Khataee & S. Karaca, "Optimization of comparative removal of two structurally different basic dyes using coal as a low-cost and available adsorbent", *Journal of the Taiwan Institute of Chemical Engineers,* 45, 4, pp. 1597-1607, 2014. Doi:10.1016/j.jtice.2013.10.014.

[4] E. Ayranci & O. Duman, "In-situ UV-visible spectroscopic study on the adsorption of some dyes onto activated carbon cloth", *Separation Science and Technology,* 44, 15, pp. 3735-3752, 2009. Doi:10.1080/01496390903182891.

[5] O. Duman, S. Tunc, & T.G. Polat, "Adsorptive removal of triarylmethane dye (Basic Red 9) from aqueous solution by sepiolite as effective and low-cost adsorbent", *Microporous and Mesoporous Materials,* 210, pp. 176-184, 2015. Doi:10.1016/j.micromeso.2015.02.040.

[6] O. Duman, S. Tunç, T.G. Polat & B.K. Bozoğlan, "Synthesis of magnetic oxidized multiwalled carbon nanotube-κ-carrageenan-Fe3O4 nanocomposite adsorbent and its application in cationic Methylene Blue dye adsorption", *Carbohydrate Polymers,* 147, pp. 79-88, 2016. Doi:10.1016/j.carbpol.2016.03.099.

[7] H.A. Kiwaan, T.M. Atwee, E.A. Azab& A.A. El-Bindary, "Photocatalytic degradation of organic dyes in the presence of nanostructured titanium dioxide", *Journal of Molecular Structure,* 1200, pp. 127115, 2020. Doi:10.1016/j.molstruc.2019.127115.

[8] M. Daraee, E. Ghasemy & A. Rashidi, "Effective adsorption of hydrogen sulfide by intercalation of

$TiO_2$ and N-doped $TiO_2$ in graphene oxide", *Journal of Environmental Chemical Engineering,* 8, 4, pp. 103836, 2020. Doi:10.1016/j.jece.2020.103836.

[9] N. Riaz, F.K. Chong, Z.B. Man, M.S. Khan & B.K. Dutta, "Photodegradation of orange II under visible light using Cu–Ni/$TiO_2$: Influence of Cu: Ni mass composition, preparation, and calcination temperature", *Industrial & Engineering Chemistry Research,* 52, 12, pp. 4491-4503, 2013. Doi:10.1021/ie303255v.

[10] I. Khan, K. Saeed, N. Ali, I. Khan, B. Zhang & M. Sadiq, "Heterogeneous photodegradation of industrial dyes: An insight to different mechanisms and rate affecting parameters", *Journal of Environmental Chemical Engineering,* 8, 5, pp. 104364, 2020. Doi:10.1016/j.jece.2020.104364.

[11] M. Humayun, F. Raziq, A. Khan & W. Luo, "Modification strategies of $TiO_2$ for potential applications in photocatalysis: a critical review", *Green Chemistry Letters Reviews,* 11, 2, pp. 86-102, 2018. Doi:17518253.2018.1440324

[12] P. Karuppasamy, N.R.N. Nisha, A. Pugazhendhi, S. Kandasamy & S. Pitchaimuthu, "An investigation of transition metal doped $TiO_2$ photocatalysts for the enhanced photocatalytic decoloration of methylene blue dye under visible light irradiation", *Journal of Environmental Chemical Engineering,* 9, 4, pp. 105254, 2021. Doi:10.1016/j.jece.2021.105254.

[13] T. Jia, F. Fu, D. Yu, J. Cao & G. Sun, "Facile synthesis and characterization of N-doped $TiO_2$/C nanocomposites with enhanced visible-light photocatalytic performance", *Applied Surface Science,* 430, pp. 438-447, 2018. Doi:10.1016/j.apsusc.2017.07.024.

[14] X. Cheng, X. Yu, Z. Xing & L. Yang, "Synthesis and characterization of N-doped $TiO_2$ and its enhanced visible-light photocatalytic activity", *Arabian Journal of Chemistry,* 9, pp. S1706-S1711, 2016. Doi:10.1016/j.arabjc.2012.04.052.

[15] J. Huang, L. Dou, J. Li, J. Zhong, M. Li & T. Wang, "Excellent visible light responsive photocatalytic behavior of N-doped $TiO_2$ toward decontamination of organic pollutants", *Journal of Hazardous Materials,* 403, pp. 123857, 2021. Doi:10.1016/j.jhazmat.2020.123857.

[16] A. Panepinto, J. Dervaux, P. A. Cormier, M. Boujtita, F. Odobel & R. Snyders, "Synthesis of p-type N-doped $TiO_2$ thin films by co-reactive magnetron sputtering", *Plasma Processes and Polymers,* 17, 3, pp. 1900203, 2020. Doi:10.1002/ppap.201900203

[17] A. Panepinto, D. Cossement & R. Snyders, "Experimental and theoretical study of the synthesis of N-doped $TiO_2$ by N ion implantation of $TiO_2$ thin films", *Applied Surface Science,* 541, pp. 148493, 2021. Doi:10.1016/j.apsusc.2020.148493.

[18] M. Xing, J. Zhang & F. Chen, "New approaches to prepare nitrogen-doped $TiO_2$ photocatalysts and study on their photocatalytic activities in visible light," *Applied Catalysis B: Environmental,* 89, 3-4, pp. 563-569, 2009. Doi:10.1016/j.apcatb.2009.01.016

[19] A. Panepinto, D. Cornil, P. Guttmann, C. Bittencourt, J. Cornil, & R. Snyders, "Fine Control of the Chemistry of Nitrogen Doping in $TiO_2$: A Joint Experimental and Theoretical Study", *The Journal of Physical Chemistry C,* 124, 31, pp. 17401-17412, 2020. Doi: 10.1021/acs.jpcc.0c05003

[20] D.A. Agyeman, K. Song, S.H. Kang, M.R. Jo, E. Cho & Y.-M. Kang, "An improved catalytic effect of nitrogen-doped $TiO_2$ nanofibers for rechargeable Li–$O_2$ batteries; the role of oxidation states and vacancies on the surface", *Journal of Materials Chemistry A,* 3, 45, pp. 22557-22563, 2015. Doi:10.1039/C5TA05426E

[21] C. Bittencourt, M. Rutar, P. Umek, A. Mrzel, K. Vozel, D. Arčon, K. Henzler, P. Krüger, & P. Guttmann, Molecular nitrogen in N-doped $TiO_2$ nanoribbons", *RSC Advances,* 5, 30, pp. 23350-23356, 2015. Doi:10.1039/C4RA14410D

[22] B. Tryba, M. Wozniak, G. Zolnierkiewicz, N. Guskos, A. Morawski, C. Colbeau-Justin, R. Wrobel, A. Nitta & B. Ohtani, "Influence of an electronic structure of N-$TiO_2$ on its photocatalytic activity towards decomposition of acetaldehyde under UV and fluorescent lamps irradiation", *Catalysts,* 8, 2, pp. 85, 2018. Doi:10.3390/catal8020085

[23] C. Di Valentin, G. Pacchioni, A. Selloni, S. Livraghi & E. Giamello, "Characterization of paramagnetic species in N-doped $TiO_2$ powders by EPR spectroscopy and DFT calculations", *The Journal of Physical Chemistry B,* 109, 23, pp. 11414-11419, 2005. Doi:10.1021/jp051756t

[24] N. Kovalevskiy, D. Selishchev, D. Svintsitskiy, S. Selishcheva, A. Berezin & D. Kozlov, "Synergistic effect of polychromatic radiation on visible light activity of N-doped $TiO_2$ photocatalyst", *Catalysis*

*Communications,* 134, pp. 105841, 2020. Doi:10.1016/j.catcom.2019.105841.

[22] D. Ma, J. Zhong, J. Li, C. Burda & R. Duan, "Preparation and photocatalytic performance of MWCNTs/BiOCl: Evidence for the superoxide radical participation in the degradation mechanism of phenol", *Applied Surface Science,* 480, pp. 395-403, 2019. Doi: 10.1016/j.apsusc.2019.02.195

[26] D. Xu, Z.-H. Huang, F. Kang, M. Inagaki, & T. H. Ko, "Effect of heat treatment on adsorption performance and photocatalytic activity of $TiO_2$-mounted activated carbon cloths", *Catalysis Today,* 139, 1, pp. 64-68, 2008. 10.1016/j.cattod.2008.08.009.

[27] G. Zhang, Y. Liu, Z. Hashisho, Z. Sun, S. Zheng, & L. Zhong, "Adsorption and photocatalytic degradation performances of $TiO_2$/diatomite composite for volatile organic compounds: Effects of key parameters", *Applied Surface Science,* 525, pp. 146633, 2020. Doi:10.1016/j.apsusc.2020.146633.

[28] F. Jiang, S. Zheng, L. An, & H. Chen, "Effect of calcination temperature on the adsorption and photocatalytic activity of hydrothermally synthesized $TiO_2$ nanotubes", *Applied surface Science,* 258, 18, pp. 7188-7194, 2012. Doi:10.1016/j.apsusc.2012.04.032

[29] M. R. Al-Mamun, S. Kader, M. S. Islam, & M. Z. H. Khan, "Photocatalytic activity improvement and application of UV-$TiO_2$ photocatalysis in textile wastewater treatment: A review", *Journal of Environmental Chemical Engineering,* 7, 5, pp. 103248, 2019. Doi:10.1016/j.jece.2019.103248.

[30] M. Bellardita, A. Di Paola, B. Megna, & L. Palmisano, "Determination of the crystallinity of $TiO_2$ photocatalysts", *Journal of Photochemistry and Photobiology A: Chemistry,* 367, pp. 312-320, 2018. Doi:10.1016/j.jphotochem.2018.08.042.